In Vivo HIF-Mediated Reductive Carboxylation Is Regulated by Citrate Levels and Sensitizes *VHL*-Deficient Cells to Glutamine Deprivation

Paulo A. Gameiro,[1,2,4,5] Juanjuan Yang,[1,2] Ana M. Metelo,[1,2] Rocio Pérez-Carro,[7] Rania Baker,[1,2] Zongwei Wang,[3] Alexandra Arreola,[6] W. Kimryn Rathmell,[6] Aria Olumi,[3] Pilar López-Larrubia,[7] Gregory Stephanopoulos,[4] and Othon Iliopoulos[1,2,*]

[1]Center for Cancer Research, Massachusetts General Hospital Cancer Center, Charlestown, MA 02129, USA
[2]Division of Hematology/Oncology, Department of Medicine
[3]Department of Urology
Massachusetts General Hospital, Boston, MA 02114, USA
[4]Department of Chemical Engineering, Massachusetts Institute of Technology, Cambridge, MA 02139, USA
[5]Department of Life Sciences, University of Coimbra, 3004-517 Coimbra, Portugal
[6]UNC Lineberger Comprehensive Cancer Center, Departments of Medicine and Genetics, University of North Carolina, Chapel Hill, NC, USA
[7]Instituto de Investigaciones Biomédicas "Alberto Sols," CSIC-UAM, 28029 Madrid, Spain
*Correspondence: oiliopoulos@partners.org
http://dx.doi.org/10.1016/j.cmet.2013.02.002

SUMMARY

Hypoxic and *VHL*-deficient cells use glutamine to generate citrate and lipids through reductive carboxylation (RC) of α-ketoglutarate. To gain insights into the role of HIF and the molecular mechanisms underlying RC, we took advantage of a panel of disease-associated *VHL* mutants and showed that HIF expression is necessary and sufficient for the induction of RC in human renal cell carcinoma (RCC) cells. HIF expression drastically reduced intracellular citrate levels. Feeding *VHL*-deficient RCC cells with acetate or citrate or knocking down PDK-1 and ACLY restored citrate levels and suppressed RC. These data suggest that HIF-induced low intracellular citrate levels promote the reductive flux by mass action to maintain lipogenesis. Using [$1-^{13}$C] glutamine, we demonstrated in vivo RC activity in *VHL*-deficient tumors growing as xenografts in mice. Lastly, HIF rendered *VHL*-deficient cells sensitive to glutamine deprivation in vitro, and systemic administration of glutaminase inhibitors suppressed the growth of RCC cells as mice xenografts.

INTRODUCTION

Cancer cells undergo fundamental changes in their metabolism to support rapid growth, adapt to limited nutrient resources, and compete for these supplies with surrounding normal cells. One of the metabolic hallmarks of cancer is the activation of glycolysis and lactate production even in the presence of adequate oxygen. This is termed the Warburg effect, and efforts in cancer biology have revealed some of the molecular mechanisms responsible for this phenotype (Cairns et al., 2011). More recently, ^{13}C isotopic studies have elucidated the complementary switch of glutamine metabolism that supports efficient

carbon utilization for anabolism and growth (DeBerardinis and Cheng, 2010). Acetyl-CoA is a central biosynthetic precursor for lipid synthesis, being generated from glucose-derived citrate in well-oxygenated cells (Hatzivassiliou et al., 2005). Warburg-like cells, and those exposed to hypoxia, divert glucose to lactate, raising the question of how the tricarboxylic acid (TCA) cycle is supplied with acetyl-CoA to support lipogenesis. We and others demonstrated, using ^{13}C isotopic tracers, that cells under hypoxic conditions or defective mitochondria primarily utilize glutamine to generate citrate and lipids through reductive carboxylation (RC) of α-ketoglutarate by isocitrate dehydrogenase 1 (IDH1) or 2 (IDH2) (Filipp et al., 2012; Metallo et al., 2012; Mullen et al., 2012; Wise et al., 2011).

The transcription factors hypoxia inducible factors 1α and 2α (HIF-1α, HIF-2α) have been established as master regulators of the hypoxic program and tumor phenotype (Gordan and Simon, 2007; Semenza, 2010). In addition to tumor-associated hypoxia, HIF can be directly activated by cancer-associated mutations. The von Hippel-Lindau (*VHL*) tumor suppressor is inactivated in the majority of sporadic clear-cell renal carcinomas (RCC), with *VHL*-deficient RCC cells exhibiting constitutive HIF-1α and/or HIF-2α activity irrespective of oxygen availability (Kim and Kaelin, 2003). Previously, we showed that *VHL*-deficient cells also relied on RC for lipid synthesis even under normoxia. Moreover, metabolic profiling of two isogenic clones that differ in pVHL expression (WT8 and PRC3) suggested that reintroduction of wild-type *VHL* can restore glucose utilization for lipogenesis (Metallo et al., 2012). The *VHL* tumor suppressor protein (pVHL) has been reported to have several functions other than the well-studied targeting of HIF. Specifically, it has been reported that pVHL regulates the large subunit of RNA polymerase (Pol) II (Mikhaylova et al., 2008), p53 (Roe et al., 2006), and the Wnt signaling regulator Jade-1. *VHL* has also been implicated in regulation of NF-κB signaling, tubulin polymerization, cilia biogenesis, and proper assembly of extracellular fibronectin (Chitalia et al., 2008; Kim and Kaelin, 2003; Ohh et al., 1998; Thoma et al., 2007; Yang et al., 2007). Hypoxia inactivates the α-ketoglutarate-dependent HIF prolyl hydroxylases, leading to

stabilization of HIF. In addition to this well-established function, oxygen tension regulates a larger family of α-ketoglutarate-dependent cellular oxygenases, leading to posttranslational modification of several substrates, among which are chromatin modifiers (Melvin and Rocha, 2012). It is therefore conceivable that the effect of hypoxia on RC that was reported previously may be mediated by signaling mechanisms independent of the disruption of the pVHL-HIF interaction. Here we (1) demonstrate that HIF is necessary and sufficient for RC, (2) provide insights into the molecular mechanisms that link HIF to RC, (3) detected RC activity in vivo in human *VHL*-deficient RCC cells growing as tumors in nude mice, (4) provide evidence that the reductive phenotype of *VHL*-deficient cells renders them sensitive to glutamine restriction in vitro, and (5) show that inhibition of glutaminase suppresses growth of *VHL*-deficient cells in nude mice. These observations lay the ground for metabolism-based therapeutic strategies for targeting HIF-driven tumors (such as RCC) and possibly the hypoxic compartment of solid tumors in general.

RESULTS

Functional Interaction between pVHL and HIF Is Necessary to Inhibit RC

To test whether the inhibition of RC by pVHL requires its ability to bind and inactivate the alpha regulatory subunit of HIF, we tested a panel of *VHL* germline mutations that are linked to different clinical phenotypes of the VHL disease and differ in their affinity to bind HIF. Missense germline type 2A *VHL* mutations confer a low risk for RCC to their carrier individuals and retain an attenuated HIF binding and regulatory activity. In contrast, type 2B mutations, which are defective in HIF binding and regulation, confer a high risk for RCC. On the other hand, type 2C *VHL* germline mutations are associated with an increased risk of pheochromocytomas, but not RCC, and they retain the ability to bind and inactivate HIF in a manner similar to wild-type protein, an observation that suggests that type 2C mutations inactivate HIF-independent function(s) of pVHL (Li et al., 2007).

We infected *VHL*-deficient human UMRC2 renal carcinoma cells with retroviruses and generated polyclonal cell populations expressing wild-type pVHL or type 2A (Y112H), type 2B (Y98N, Y112N), and type 2C (L188V) pVHL mutants. First, we confirmed that expression of HIF-1α/HIF-2α and their downstream target GLUT1 were downregulated in cells expressing wild-type pVHL or type 2C mutant protein (Figure 1A). The effect of type 2A pVHL mutations appeared intermediate between wild-type and type 2B mutations regarding GLUT1 (Figure 1A, GLUT1 lane).

To profile the metabolic phenotype of the engineered cell lines, we labeled the cells with either [U^{13}-C$_6$]glucose or [1-^{13}C$_1$]glutamine and determined the incorporation of each tracer in TCA cycle metabolites using gas chromatography-mass spectrometry (GC-MS) (Figure 1B). Reintroduction of wild-type pVHL or type 2C pVHL mutant suppressed the contribution of reductive carboxylation from glutamine (Figure 1C), as determined by the degree of labeled carbon (M1 enrichment) of the indicated metabolites (see Figure 1B, green circles). Conversely, type 2B mutants (Y112N/Y98N, which are defective in HIF inactivation) exhibited active RC to a level comparable to *VHL*-deficient control cells. We observed a concurrent regulation in glucose metabolism in the different *VHL* mutants. Reintroduc-

tion of wild-type or type 2C pVHL mutant, which can mediate HIF-α destruction, stimulated glucose oxidation via pyruvate dehydrogenase (PDH), as determined by the degree of ^{13}C-labeled TCA cycle metabolites (M2 enrichment) (Figures 1D and 1E). In contrast, reintroduction of an HIF nonbinding Type 2B pVHL mutant failed to stimulate glucose oxidation, resembling the phenotype observed in *VHL*-deficient cells (Figures 1D and 1E). Additional evidence for the overall glucose utilization was obtained from the enrichment of M3 isotopomers using [U^{13}-C$_6$]glucose (Figure S1A), which shows a lower contribution of glucose-derived carbons to the TCA cycle in *VHL*-deficient RCC cells (via pyruvate carboxylase and/or continued TCA cycling).

To test the effect of HIF activation on the overall glutamine incorporation in the TCA cycle, we labeled an isogenic pair of *VHL*-deficient and *VHL*-reconstituted UMRC2 cells with [U-^{13}C$_5$]glutamine, which generates M4 fumarate, M4 malate, M4 aspartate, and M4 citrate isotopomers through glutamine oxidation. As seen in Figure S1B, *VHL*-deficient/*VHL*-positive UMRC2 cells exhibit similar enrichment of M4 fumarate, M4 malate, and M4 asparate (but not citrate) showing that *VHL*-deficient cells upregulate reductive carboxylation without compromising oxidative metabolism from glutamine. Next, we tested whether HIF inactivation by pVHL is necessary to regulate the reductive utilization of glutamine for lipogenesis. To this end, we traced the relative incorporation of [U-^{13}C$_6$]glucose or [5-^{13}C$_1$]glutamine into palmitate. Labeled carbon derived from [5-^{13}C$_1$]glutamine can be incorporated into fatty acids exclusively through RC, and the labeled carbon cannot be transferred to palmitate through the oxidative TCA cycle (Figure 1B, red carbons). Tracer incorporation from [5-^{13}C$_1$]glutamine occurs in the one carbon (C1) of acetyl-CoA, which results in labeling of palmitate at M1, M2, M3, M4, M5, M6, M7, and M8 mass isotopomers. In contrast, lipogenic acetyl-CoA molecules originating from [U-^{13}C$_6$]glucose are fully labeled, and the labeled palmitate is represented by M2, M4, M6, M8, M10, M12, M14, and M16 mass isotopomers. *VHL*-deficient control cells and cells expressing pVHL type 2B mutants exhibited high palmitate labeling from the [5-^{13}C$_1$]glutamine; conversely, reintroduction of wild-type or type 2C pVHL mutant (L188V) resulted in high labeling from [U-^{13}C$_6$]glucose (Figures 2A and 2B, box inserts highlight the heavier mass isotopomers).

Next, to determine the specific contribution from glucose oxidation or glutamine reduction to lipogenic acetyl-CoA, we performed isotopomer spectral analysis (ISA) of palmitate labeling patterns. ISA indicates that wild-type pVHL or pVHL L188V mutant-reconstituted UMRC2 cells relied mainly on glucose oxidation to produce lipogenic acetyl-CoA, while UMRC2 cells reconstituted with a pVHL mutant defective in HIF inactivation (Y112N or Y98N) primarily employed RC. Upon disruption of the pVHL-HIF interaction, glutamine becomes the preferred substrate for lipogenesis, supplying 70%–80% of the lipogenic acetyl-CoA (Figure 2C). This is not a cell-line-specific phenomenon, but it applies to *VHL*-deficient human RCC cells in general; the same changes are observed in 786-O cells reconstituted with wild-type pVHL or mutant pVHL or infected with vector only as control (Figure S2). Type 2A pVHL mutants (Y112H, which retain partial HIF binding) confer an intermediate reductive phenotype between wild-type VHL (which inactivates HIF) and type 2B
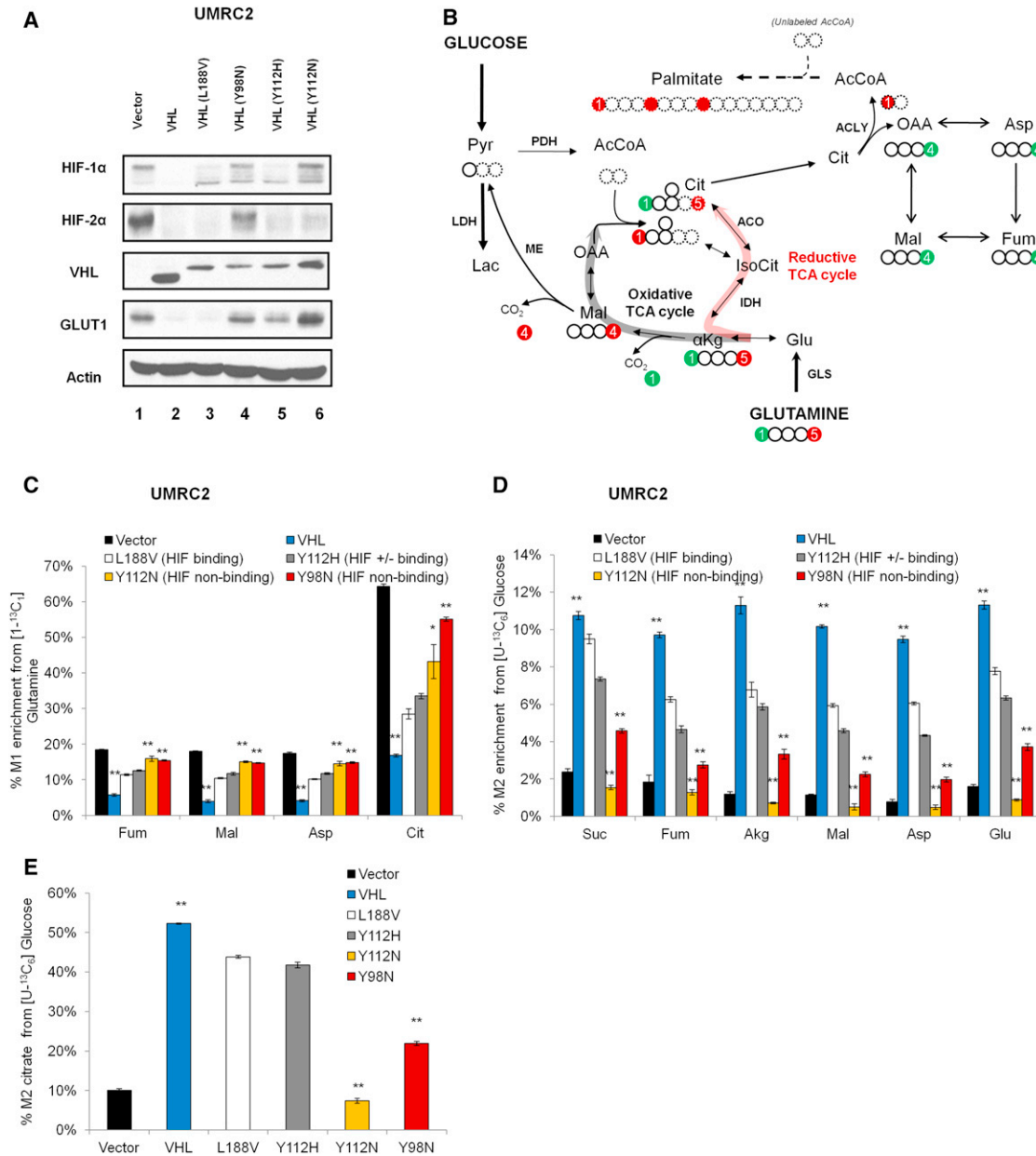
Figure 1. HIF Inactivation Is Necessary for Downregulation of Reductive Carboxylation by pVHL

(A) Expression of HIF-1 α, HIF-2α, and their target protein GLUT1 in UMRC2-derived cell lines, as indicated.

(B) Carbon atom transition map: the fate of [1-$^{13}C_1$] and [5-$^{13}C_1$]glutamine used to trace reductive carboxylation in this work (carbon atoms are represented by circles). The [1-$^{13}C_1$] (green circle) and [5-$^{13}C_1$] (red circle) glutamine-derived isotopic labels are retained during the reductive TCA cycle (bold red pathway). Metabolites containing the acetyl-CoA carbon skeleton are highlighted by dashed circles.

(C) Relative contribution of reductive carboxylation.

(D and E) Relative contribution of glucose oxidation to the carbons of indicated metabolites (D) and citrate (E). Student's t test compared *VHL*-reconstituted to vector-only or to *VHL* mutants (Y98N/Y112N). Error bars represent SEM. Pyr, pyruvate; Lac, lactate; AcCoA, acetyl-CoA, Cit, citrate; IsoCit, isocitrate; Akg, α-ketoglutarate; Suc, succinate; Fum, fumarate; Mal, malate; OAA, oxaloacetate; Asp, aspartate; Glu, glutamate; PDH, pyruvate dehydrogenase; ME, malic enzyme; IDH, isocitrate dehydrogenase enzymes; ACO, aconitase enzymes; ACLY, ATP-citrate lyase; GLS, glutaminase. See also Figure S1.

pVHL mutants (which are totally defective in HIF regulation) as seen in Figures 1 and 2. Taken together, these data demonstrate that the ability of pVHL to regulate reductive carboxylation and lipogenesis from glutamine tracks genetically with its ability to bind and degrade HIF, at least in RCC cells.

HIF Is Sufficient to Induce RC from Glutamine in RCC Cells

To test the hypothesis that HIF-2α is sufficient to promote RC from glutamine, we expressed a pVHL-insensitive HIF-2α mutant (HIF-2α P405A/P531A, marked as HIF-2α P-A) in
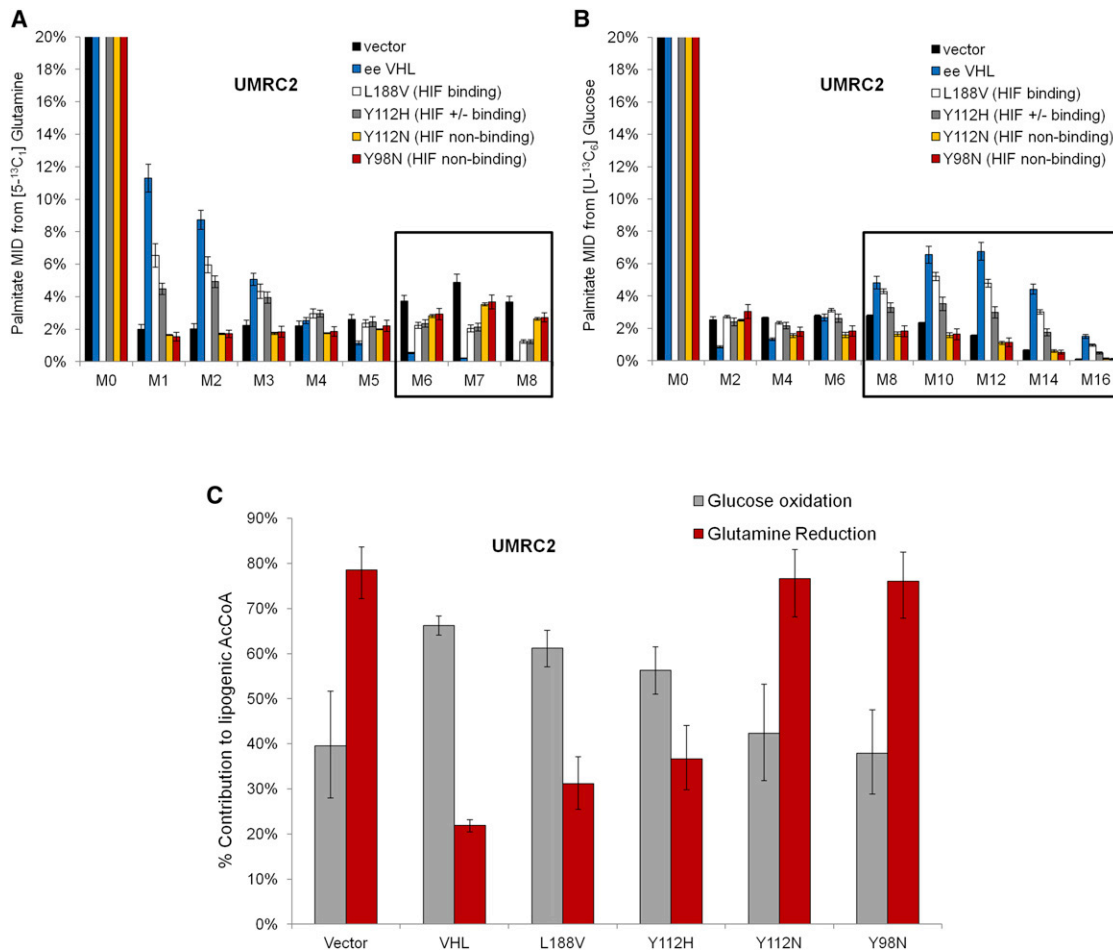
Figure 2. HIF Inactivation Is Necessary for Downregulation of Reductive Lipogenesis by pVHL

(A and B) *VHL*-deficient UMRC2 cells were cultured for 3 days in the presence of either [U-$^{13}C_6$]glucose or [5-$^{13}C_1$]glutamine. Mass isotopomer distributions (MIDs) of biomass-extracted palmitate in parental cells reconstituted with empty vector control (vector), wild-type EE-VHL, or HA-VHL mutants and labeled with [5-$^{13}C_1$]glutamine (A) or [U-$^{13}C_6$]glucose (B). Note: M0 equals 70%–80%; scale shown up to 20%. Error bars represent SEM.

(C) Specific contribution to lipogenic acetyl-CoA as estimated by the ISA method. Error bars represent 95% confidence intervals. See also Figure S2.

VHL-reconstituted 786-O cells (Figure 3). HIF-2α P-A is constitutively expressed in this polyclonal cell population, despite the reintroduction of wild-type *VHL*, reflecting a pseudohypoxia condition (Figure 3A). We confirmed that this mutant is transcriptionally active by assaying for the expression of its targets genes GLUT1, LDHA, HK1, EGLN, HIG2, and VEGF (Figures 3B and S3A). As shown in Figure 3C, reintroduction of wild-type *VHL* into 786-O cells suppressed RC, whereas the expression of the constitutively active HIF-2α mutant was sufficient to stimulate this reaction, restoring the M1 enrichment of TCA cycle metabolites observed in *VHL*-deficient 786-O cells. Expression of HIF-2α P-A also led to a concomitant decrease in glucose oxidation, corroborating the metabolic alterations observed in glutamine metabolism (Figures 3D and 3E). Additional evidence of the HIF2α-regulation on the reductive phenotype was obtained with [U-$^{13}C_5$]glutamine, which generates M5 citrate, M3 fumarate, M3 malate, and M3 aspartate through RC (Figure 3F).

Next, we tested whether *VHL*-independent HIF-2α expression was sufficient not only to stimulate RC in the TCA cycle but also

to switch the substrate preference for lipogenesis from glucose to glutamine. Expression of HIF-2α P-A in 786-O cells phenocopied the loss-of-*VHL* with regards to glutamine reduction for lipogenesis (Figure 3G), suggesting that HIF-2α can induce the glutamine-to-lipid pathway in RCC cells per se. Although reintroduction of wild-type *VHL* restored glucose oxidation in UMRC2 and UMRC3 cells (Figures S3B–S3I), HIF-2α P-A expression did not measurably affect the contribution of each substrate to the TCA cycle or lipid synthesis in these RCC cells (data not shown). UMRC2 and UMRC3 cells endogenously express both HIF-1α and HIF-2α, whereas 786-O cells exclusively express HIF-2α. There is compelling evidence suggesting, at least in RCC cells, that HIF-α isoforms have overlapping—but also distinct—functions and their roles in regulating bioenergetic processes remain an area of active investigation. Overall, HIF-1α has an antiproliferative effect, and its expression in vitro leads to rapid death of RCC cells while HIF-2α promotes tumor growth (Keith et al., 2011; Raval et al., 2005). Because of this, we were not able to stably express the HIF-1α P-A mutant in cells that endogenously express HIF-2α only. To get insights into the
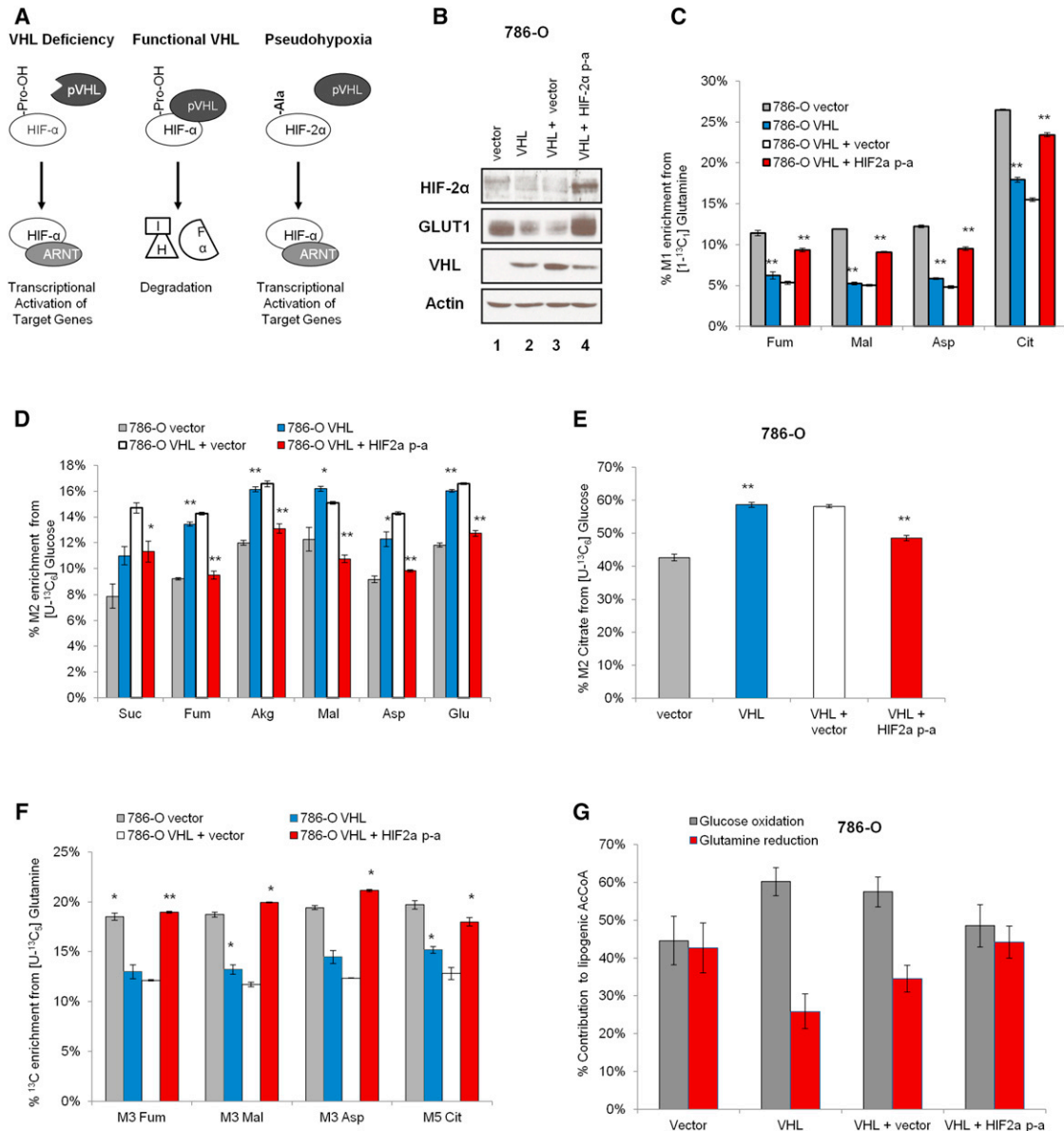
Figure 3. Expression of HIF-2α Is Sufficient to Induce Reductive Carboxylation and Lipogenesis from Glutamine in RCC Cells

(A) Schematic of stabilized HIF-2α expression under normoxia conditions.

(B) Expression of pVHL, HIF-2α, and its target protein GLUT1 in 786-O-derived cells, as indicated.

(C) Relative contribution of reductive carboxylation.

(D and E) Relative contribution of glucose oxidation to the carbons of indicated metabolites (D) and citrate (E).

(F) Evidence for induction of reductive carboxylation by HIF-2α P-A using [U-^{13}C$_5$]glutamine. Student's t test compared VHL-reconstituted or mutant HIF-2α-expressing cells to corresponding controls. Error bars represent SEM.

(G) ISA results showing the specific contribution of glucose oxidation and glutamine reduction to lipogenic acetyl-CoA (error bars denote 95% confidence intervals). See also Figure S3.

role of HIF-α paralogs in promoting RC, we used mouse neonatal epithelial kidney (NEK) cells and selectively induced the expression of mouse HIF-1α or HIF-2α P-A in normoxia. Expressing HIF-1α P-A activated RC, consistent with our observation in cancer cell lines. In this model, HIF-2α P-A did not affect the contribution of this reaction to any of the TCA cycle metabolites, at least in the condition studied (Figure S3J). Thus, it is possible that the induction of RC by HIF-1α or HIF-2α is species- or cell-

type-specific. Alternatively, there may be a redundant role of the paralogs, and/or one may adapt the control of the metabolic program in the absence of the other paralog.

Metabolic Flux Analysis Shows Net Reversion of the IDH Flux upon HIF Activation

To determine absolute fluxes in RCC cells, we employed ^{13}C metabolic flux analysis (MFA) as previously described
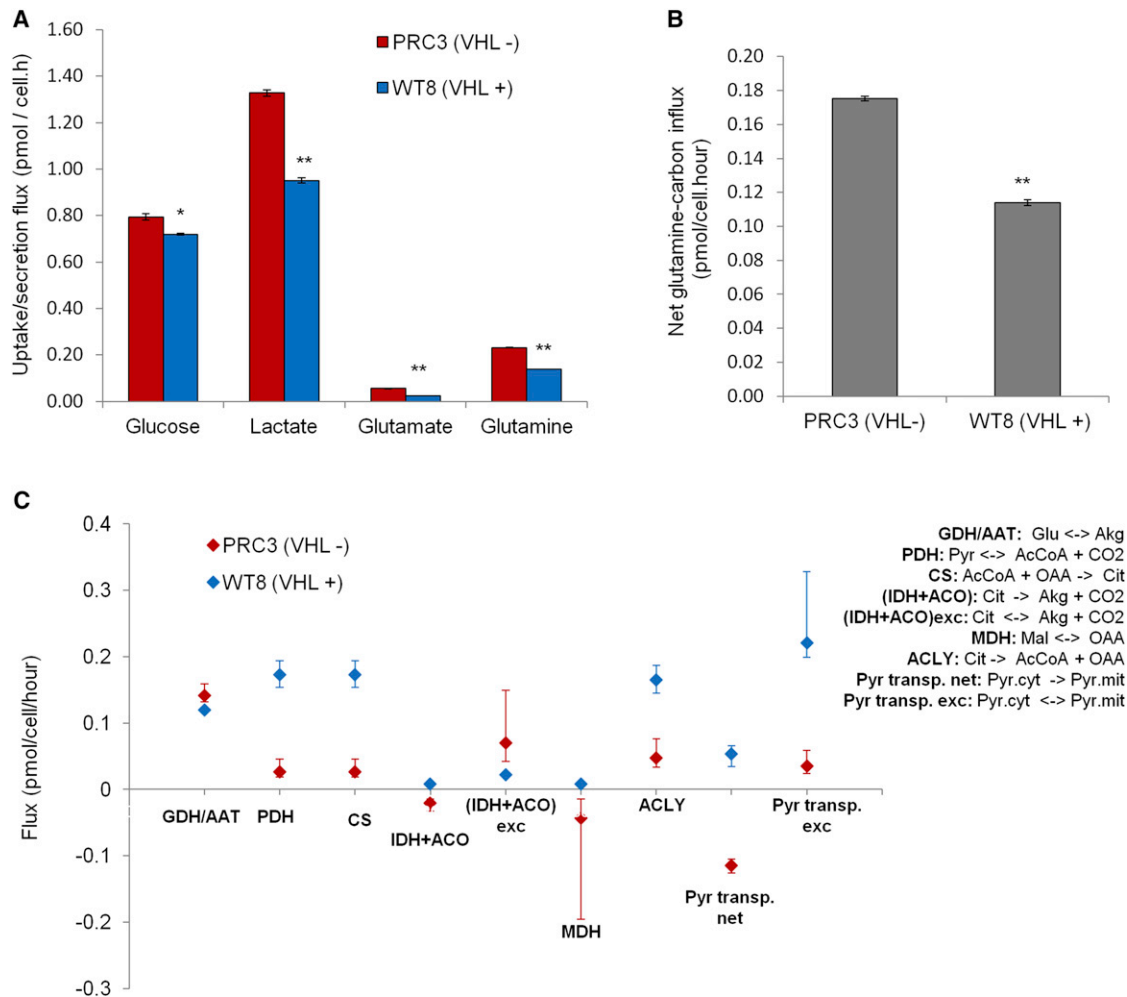
Figure 4. Metabolic Flux Analysis of *VHL*-Deficient and *VHL*-Positive Cells

(A) Extracellular fluxes (Glc and Gln uptake, Glu and lactic acid secretion) in PRC3 (VHL$^{-/-}$) and WT8 (VHL^{+}) isogenic cells. Error bars denote SEM.

(B) Net influx of glutamine-derived carbons determined by the difference between glutamine uptake and glutamate secretion. Error bars denote SEM.

(C) Flux estimates from combined [U-^{13}C$_6$]glucose/[1-^{13}C$_1$]glutamine MFA model. Student's t test compared WT8 to PRC3 cells. GDH, glutamate dehydrogenase; AAT, aspartate aminotransferase; PDH, pyruvate dehydrogenase; CS, citrate synthase; IDH, isocitrate dehydrogenase; ACO, aconitase; MDH, malate dehydrogenase; ACLY, ATP-citrate lyase; Pyr transp, pyruvate transport between cytosol and mitochondria. Error bars denote 95% confidence intervals.

(Metallo et al., 2012). Herein, we performed MFA using a combined model of [U-^{13}C$_6$]glucose and [1-^{13}C$_1$]glutamine tracer data sets from the 786-O derived isogenic clones PRC3 (VHL$^{-/-}$)/WT8 (VHL^{+}) cells, which show a robust metabolic regulation by reintroduction of pVHL. To this end, we first determined specific glucose/glutamine consumption and lactate/glutamate secretion rates. As expected, PRC3 exhibited increased glucose consumption and lactate production when compared to WT8 counterparts (Figure 4A). While PRC3 exhibited both higher glutamine consumption and glutamate production rates than WT8 (Figure 4A), the net carbon influx was higher in PRC3 cells (Figure 4B). Importantly, the fitted data show that the flux of citrate to α-ketoglutarate was negative in PRC3 cells (Figure 4C). This indicates that the net (forward plus reverse) flux of isocitrate dehydrogenase and aconitase (IDH + ACO) is toward citrate production. The exchange flux was also higher in PRC3 than WT8 cells, whereas the PDH flux was lower in PRC3 cells. In

agreement with the tracer data, these MFA results strongly suggest that the reverse IDH + ACO fluxes surpass the forward flux in *VHL*-deficient cells. The estimated ATP citrate lyase (ACLY) flux was also lower in PRC3 than in WT8 cells. Furthermore, the malate dehydrogenase (MDH) flux was negative, reflecting a net conversion of oxaloacetate into malate in *VHL*-deficient cells (Figure 4C). This indicates an increased flux through the reductive pathway downstream of IDH, ACO, and ACLY. Additionally, some TCA cycle flux estimates downstream of α-ketoglutarate were not significantly different between PRC and WT8 (Table S1). This shows that *VHL*-deficient cells maintain glutamine oxidation while upregulating reductive carboxylation (Figure S1B). This finding is in agreement with the higher glutamine uptake observed in *VHL*-deficient cells. Table S1 shows the metabolic network and complete MFA results. Similar MFA results were obtained in *VHL*-deficient vector versus *VHL*-reconstituted UMRC2 cells (data not shown). Together, the MFA data
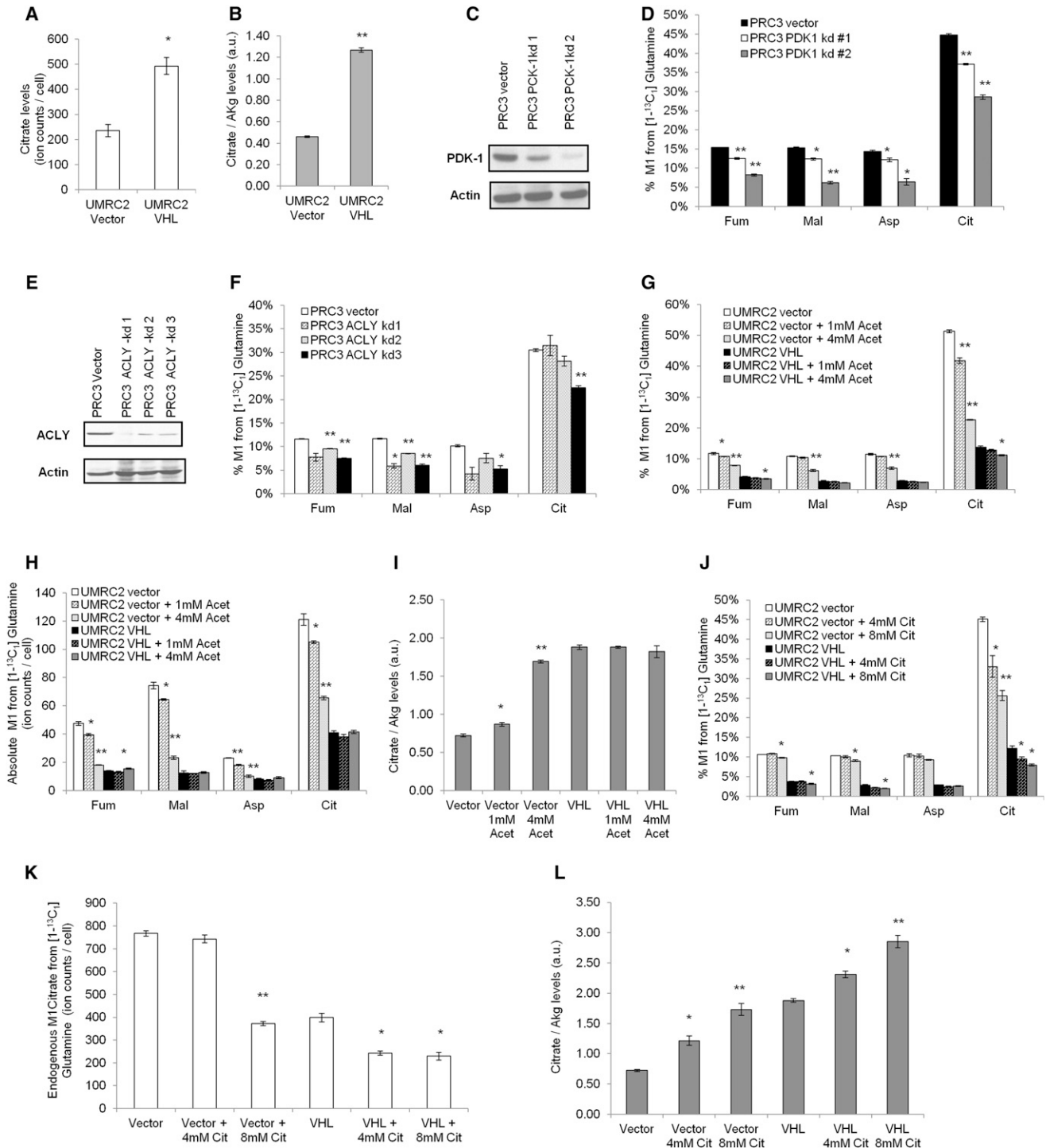
Figure 5. Regulation of HIF-Mediated Reductive Carboxylation by Citrate Levels

(A and B) Citrate ion counts (A) and citrate-to-α-ketoglutarate ratio (B) in RCC cells. Student's t test compared VHL-reconstituted to VHL-deficient cells.

(C) Validation of PDK-1 knockdown in *VHL*-deficient PRC3 cells.

(D) Relative contribution of reductive carboxylation to the TCA cycle under PDK-1 knockdown conditions. Student's t test compared PDK-1 knockdown to control cells.

(E) Validation of ACLY knockdown in PRC3 cells.

(F) Effect of ACLY knockdown on the relative contribution of reductive carboxylation. Student's t test compared ACLY knockdown to control cells.

(G and H) Effect of acetate and citrate on the activity of reductive carboxylation in VHL-deficient/VHL-reconstituted UMRC2 cells. Acetate suppresses the relative (G) and total (H) contribution of reductive carboxylation in VHL-deficient UMRC2 cells.

(legend continued on next page)

show that HIF expression reverses the net IDH flux, perhaps to compensate for a deficient citrate production due to inhibition of PDH.

HIF Activation Promotes RC by Lowering Citrate Levels

In support of the existing literature, our MFA data showed that HIF inhibits the absolute pyruvate dehydrogenase (PDH) flux (Kim et al., 2006; Papandreou et al., 2006). We observed that citrate levels were depleted in *VHL*-deficient UMRC2 cells (Figure 5A), with the citrate-to-α-ketoglutarate ratio being equally decreased in the *VHL*-deficient and HIF-2α P-A-expressing RCC cell lines (Figures 5B and S4A). We hypothesized that low citrate levels are key in promoting RC through mass action. To test if the mechanism by which HIF promotes RC lies in its ability to reduce citrate levels, we restored the intracellular pools of citrate, hoping to suppress RC in the TCA cycle. First, we knocked down the HIF target PDK-1 (Figure 5C) and observed a decreased contribution of RC to the TCA cycle in *VHL*-deficient PRC3 cells (Figure 5D). Similarly, knocking down the ATP citrate lyase enzyme (Figure 5E) inhibited RC in PRC3 cells (relative contribution of RC in Figure 5F, total contribution of RC in Figure S4B). Next, we labeled *VHL*-deficient and *VHL*-reconstituted UMRC2 cells with [1-^{13}C$_1$]glutamine and supplemented the medium with 1 mM and 4 mM acetate. Addition of acetate decreased the relative (Figure 5G) and total contribution (Figure 5H) of RC in *VHL*-deficient cells, with minimal effects observed in the V*HL*-reconstituted counterparts. The M1 enrichment informs on RC for the formation of TCA cycle metabolites. The absence of a major effect of acetate on the minimal RC of *VHL*-reconstituted cells is consistent with the observation that addition of acetate to these cells did not increase the intracellular citrate levels significantly (Figures 5I and S4C). In contrast, addition of acetate to *VHL*-deficient cells led to a significant increase in their citrate levels (Figures 5I and S4C) (to a level similar to the one observed in *VHL*-positive cells) as well as significant inhibition of RC. To pinpoint the metabolic route of the acetate-to-citrate flux, we labeled the control and ACLY knockdown PRC3 cells with [U-^{13}C$_2$]acetate and observed an increased percentage of M2 citrate under ACLY knockdown conditions (Figure S4D), suggesting that the acetate rescue of citrate levels in *VHL*-deficient cells probably occurs through condensation with oxaloacetate via citrate synthase rather than through the reversibility of ACLY. We confirmed that acetate can serve as a lipogenic source in the pair of PRC3/WT8 cells (Figure S4E). We also cultured PRC3/WT8 cells with [5-^{13}C$_1$]glutamine in the presence of naturally labeled acetate. In line with the previous observations, the contribution of glutamine reduction to lipogenic acetyl-CoA was decreased under the presence of acetate (Figure S4F). Next, we directly supplemented the medium with citrate and rinsed the cells thoroughly with PBS before extraction to ensure measurement of the intracellular metabolite. Addition of 8 mM citrate decreased the M1 enrichment of citrate in *VHL*-deficient UMRC2 cells to half but, in contrast to acetate, did have a moderate effect on

the minimal RC observed in *VHL*-reconstituted cells (Figure 5J). Interestingly the level of M1 fumarate, M1 aspartate, and M1 malate were unaffected. One could expect the addition of nonlabeled citrate to decrease, by definition, the percent enrichment of M1 citrate, regardless of its putative effect on RC. To control for this effect of exogenous citrate on the total formation of RC-derived citrate, we labeled the cells with [1-^{13}C$_1$]glutamine and [U-^{13}C$_6$]citrate and subtracted the total M6 citrate ions (which are exogenous and not metabolically generated by the cell) from the total citrate ions and calculated the total contribution of RC using the formula % M1 × (total ions−% M6 × total ions). Likewise, exogenous citrate significantly decreased the total contribution of RC in the *VHL*-deficient UMRC2 cells but also had a moderate effect in the RC observed in *VHL*-reconstituted cells (Figure 5K). This differential effect between acetate and citrate on RC is consistent with and supports our hypothesis that endogenous citrate levels regulate RC by mass action. Addition of citrate in the medium, in contrast to acetate, led to an increase in the citrate-to-α-ketoglutarate ratio (Figure 5L) and absolute citrate levels (Figure S4H) not only in *VHL*-deficient but also *VHL*-reconstituted cells. The ability of exogenous citrate, but not acetate, to also affect RC in *VHL*-reconstituted cells may be explained by compartmentalization differences or by allosteric inhibition of citrate synthase (Lehninger, 2005); that is, the ability of acetate to raise the intracellular levels of citrate may be limited in (*VHL*-reconstituted) cells that exhibit high endogenous levels of citrate. Whatever the mechanism, the results imply that increasing the pools of intracellular citrate has a direct biochemical effect in cells with regards to their reliance on RC. Finally, we assayed the transcript and protein levels of enzymes involved in the reductive utilization of glutamine and did not observe significant differences between *VHL*-deficient and *VHL*-reconstituted UMRC2 cells (Figures S4I and S4J), suggesting that HIF does not promote RC by direct transactivation of these enzymes. The IDH1/IDH2 equilibrium is defined as follows:

$$\frac{[\alpha - \text{ketoglutarate}][\text{NADPH}][\text{CO2}]}{[\text{Isocitrate}][\text{NADP}+]} = K(\text{IDH})$$

Therefore, we sought to investigate whether HIF could affect the driving force of the IDH reaction by also enhancing NADPH production. We did not observe a significant alteration of the NADP$^+$/NADPH ratio between *VHL*-deficient and VHL-positive cells in the cell lysate (Figure S4I). Yet, we determined the ratio of the free dinucleotides using the measured ratios of suitable oxidized (α-ketoglutarate) and reduced (isocitrate/citrate) metabolites that are linked to the NADP-dependent IDH enzymes. The determined ratios (Figure S4J) are in close agreement with the values initially reported by the Krebs lab (Veech et al., 1969) and showed that HIF-expressing UMRC2 cells exhibit a higher NADP$^+$/NADPH ratio. Collectively, these data strongly suggest that HIF-regulated citrate levels modulate the reductive flux to maintain adequate lipogenesis.

(I) Rescue of citrate-to-α-ketoglutarate ratio by acetate addition.

(J and K) Exogenous citrate suppresses the relative (J) and total (K) contribution of reductive carboxylation in *VHL*-deficient UMRC2 cells.

(L) Rescue of citrate-to-α-ketoglutarate ratio by exogenous citrate in (K). ACLY, ATP-citrate lyase; PDK-1, pyruvate dehydrogenase kinase. Error bars denote SEM. See also Figure S4.
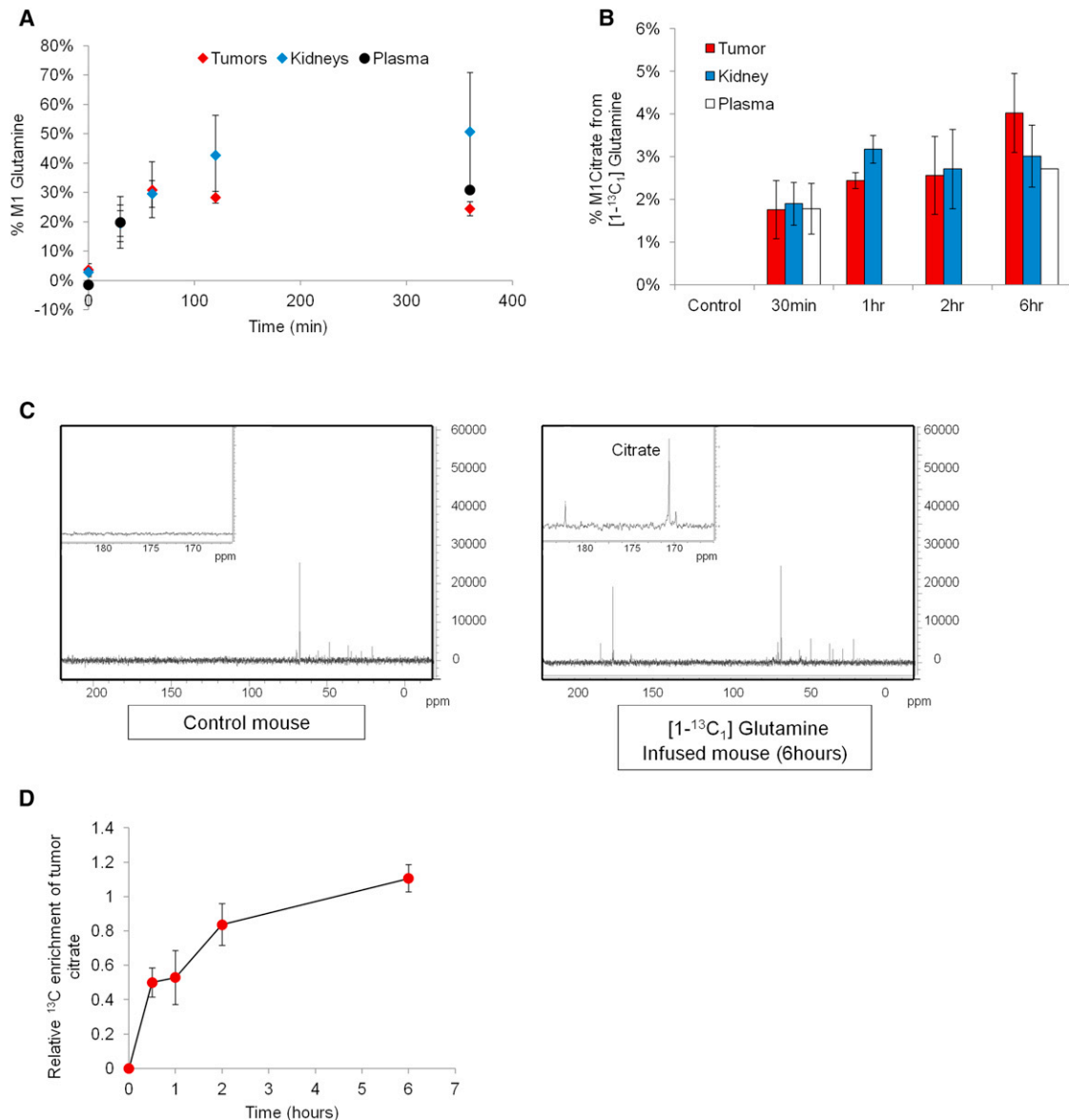
Figure 6. Evidence for Reductive Carboxylation Activity In Vivo

(A) Time course of ^{13}C enrichment (%) of glutamine in tumor, normal kidney, and plasma extracts during infusion with [1-$^{13}C_1$]glutamine. ^{13}C enrichment at time zero was determined using control noninfused mice.

(B) Percent M1 citrate in the different tissues as determined by GC-MS analysis.

(C) High-resolution ^{13}C NMR spectra showing ^{13}C enrichment of carboxylic groups in tumor extracts of a [1-$^{13}C_1$]glutamine-infused mouse when compared to a control mouse.

(D) NMR analysis of ^{13}C enrichment in tumor citrate during the time course of infusion determined by deconvolution of the carboxyl group signals. The area of the citrate signal was divided by tumor weight and normalized to the dioxane signal. Error bars represent SEM of n = 3.

Reductive Carboxylation from Glutamine Is Detectable In Vivo

VHL-deficient RCC cells rely on RC for lipid synthesis, potentially suggesting that this reaction can contribute to tumor growth. Reductive carboxylation is known to occur in bacteria and has been described in brown adipose tissue (Yoo et al., 2004) but whether it occurs in vivo in other tissues of vertebrates or in actual tumors is not known. We sought to determine the activity of RC in tumors derived from *VHL*-deficient UMRC3 cells

growing as subcutaneous xenografts in nude mice. We infused several tumor-bearing mice with [1-$^{13}C_1$]glutamine (see Experimental Procedures) and analyzed the citrate enrichment in tumor extracts by high-resolution ^{13}C nuclear magnetic resonance (NMR) spectroscopy and GC-MS (Figure 6). [1-$^{13}C_1$]glutamine will transfer carbon to citrate only through RC, so the mere detection of ^{13}C enrichment in citrate will indicate that this reaction is active in vivo. In order to attain maximal ^{13}C enrichment of citrate, we carried out a time course infusion of

[1-$^{13}C_1$]glutamine and attained an isotopic-steady state of ^{13}C glutamine enrichment in the tumor (Figure 6A). We also analyzed the ^{13}C glutamine enrichment in the plasma at the earliest and latest infusion points and observed similar ^{13}C enrichment after 6 hr. As seen in Figure 6B, we detected ^{13}C enriched citrate in the tumor within 30 min, with RC accounting for 4% of citrate production after 6 hr of infusion (Figure 6B). Notably, the steady-state ^{13}C glutamine enrichment in the tumor was 30% (Figure 6A), indicating that the reductive flux accounts for at least 12% of citrate production in *VHL*-deficient tumors under these experimental conditions. The kidney cortex is reported to be relatively hypoxic (Zhong et al., 1998). Thus, we analyzed the ^{13}C citrate enrichment in kidney extracts in parallel and showed that RC is also active in this organ (Figure 6B). The steady-state ^{13}C enrichment of glutamine was also established in the normal kidney, but it was higher (Figure 6B), indicating an overall lower contribution of RC in the kidney when compared to the tumor. Despite the steady-state ^{13}C enrichment of the glutamine precursor, the percentage of M1 citrate appeared to increase overtime in the tumor, whereas it reached a plateau in the normal kidneys and plasma. Importantly, there was no evidence that RC appears in the tumor in a delayed fashion compared to plasma or kidney, strongly suggesting that RC occurs in the tumor xenografts. Concordant results were obtained by ^{13}C NMR spectroscopy (Figures 6C and 6D) in which ^{13}C enrichment was observed in tumor extracts after 6 hr of infusion, and no signal was detected in the carboxyl group region in control mice (Figure 6C). These results indicate that RC occurs in vivo, at least in *VHL*-deficient tumors.

Loss of *VHL* Renders RCC Cells Sensitive to Glutamine Deprivation

RCC cells engaged in RC from glutamine to produce citrate, and this reaction was active in *VHL*-deficient RCC xenograft tumors. We therefore hypothesized that *VHL* deficiency results in cell addiction to glutamine for proliferation. We treated the isogenic clones PRC3 (*VHL*-deficient cells) and WT8 (*VHL*-reconstituted cells) with the glutaminase inhibitor 968 (Wang et al., 2010a). *VHL*-deficient PRC3 cells were more sensitive to treatment with 968, compared to the *VHL*-reconstituted WT8 cells (Figure 7A). To confirm that this is not only a cell-line-specific phenomenon, we also cultured UMRC2 cells in the presence of 968 or diluent control and showed selective sensitivity of *VHL*-deficient cells (Figure 7B). To test if the selective sensitivity of *VHL*-deficient cells to glutaminase inhibitors is linked, at least in part, to defective carbon supply, we asked whether cell proliferation could be rescued by anaplerotic substrates. Supplementing the cultured medium with a cell-permeable form of the substrate α-ketoglutarate or acetate, we rescued *VHL*-deficient cells from treatment with 968 (Figure 7C). The selective sensitivity and rescue by anaplerotic and lipogenic substrates was also corroborated in 786-O cells (Figure 7D). We observed a similar growth-inhibitory phenotype in *VHL*-deficient UMRC2 cells using a different glutaminase inhibitor (BPTES), confirming the sensitivity to glutamine deprivation under *VHL*-deficient conditions (Figure 7E). Glutamine addiction of *VHL*-deficient cells is not an in-vitro-only phenomenon. Systemic administration of the glutaminase inhibitor BPTES suppressed the growth of *VHL*-deficient UMRC3 cells as tumors in nude mice (Figure 7F).

In summary, our findings show that HIF is necessary and sufficient to promote RC from glutamine. By inhibiting glucose oxidation in the TCA cycle and reducing citrate levels, HIF shifts the IDH reaction toward RC to support citrate production and lipogenesis (Figure 7G). The reductive flux is active in vivo, fuels tumor growth, and can potentially be targeted pharmacologically. Understanding the significance of reductive glutamine metabolism in tumors may lead to metabolism-based therapeutic strategies.

DISCUSSION

Along with others, we reported that hypoxia and loss of *VHL* engage cells in reductive carboxylation (RC) from glutamine to support citrate and lipid synthesis (Filipp et al., 2012; Metallo et al., 2012; Wise et al., 2011). Wise et al. (2011) suggested that inactivation of HIF in VHL-deficient cells leads to reduction of RC. These observations raise the hypothesis that HIF, which is induced by hypoxia and is constitutively active in *VHL*-deficient cells, mediates RC. In our current work, we provide mechanistic insights that link HIF to RC. First, we demonstrate that polyclonal reconstitution of *VHL* in several human *VHL*-deficient RCC cell lines inhibits RC and restores glucose oxidation. Second, the *VHL* mutational analysis demonstrates that the ability of pVHL to mitigate reductive lipogenesis is mediated by HIF and is not the outcome of previously reported, HIF-independent pVHL function(s). Third, to prove our hypothesis we showed that constitutive expression of a *VHL*-independent HIF mutant is sufficient to phenocopy the reductive phenotype observed in *VHL*-deficient cells. In addition, we showed that RC is not a mere in vitro phenomenon, but it can be detected in vivo in human tumors growing as mouse xenografts. Lastly, treatment of *VHL*-deficient human xenografts with glutaminase inhibitors led to suppression of their growth as tumors.

In this work, we also examined the mechanism(s) by which HIF promotes RC. It is established that hypoxic induction of HIF transactivates several enzymes involved in glucose uptake and glycolysis, including GLUT1, hexokinase, phosphofructokinase, and aldolase (Iyer et al., 1998). In addition, HIF directly binds to the promoter of, and transactivates, PKM2, pyruvate dehydrogenase kinase 1 (PDK1) and lactate dehydrogenase A (LDHA) (Ebert et al., 1996; Firth et al., 1994; Kim et al., 2006; Luo et al., 2011; Papandreou et al., 2006). This orchestrated upregulation of several enzymes ensures the diversion of pyruvate to lactate production. This raises the hypothesis that RC may be triggered by a deficient pyruvate oxidation in the mitochondrion and the subsequent reduction in citrate levels. Our MFA analysis indicated a significantly lower absolute pyruvate dehydrogenase (PDH) flux and net conversion of α-ketoglutarate into citrate upon HIF activation. The ATP citrate lyase flux was lower in *VHL*-deficient cells when compared to the *VHL*-positive counterparts, which supports our previous observations that de novo lipogenesis is decreased under hypoxia conditions (Metallo et al., 2012). Indeed, HIF expression, either by loss of *VHL* or normoxic induction of HIF-2α P-A, reduced citrate levels. Conversely, administration of exogenous citrate or acetate in *VHL*-deficient cells restored the low citrate levels to the levels encountered in *VHL*-replete cells and inhibited RC. Exogenous
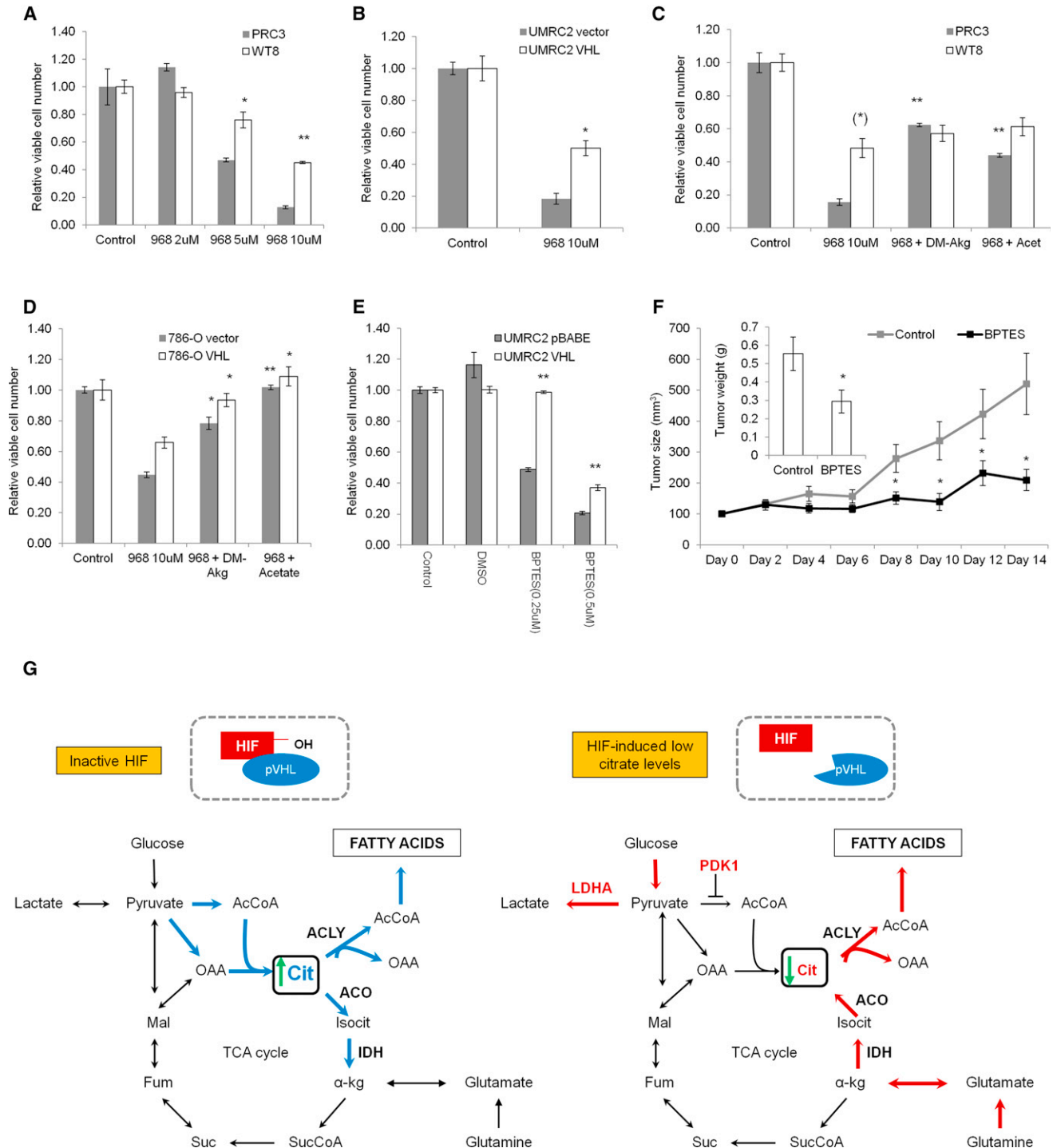
Figure 7. VHL-Deficient Cells and Tumors Are Sensitive to Glutamine Deprivation

(A–E) Cell proliferation is normalized to the corresponding cell type grown in 1 mM glutamine-containing medium. Effect of treatment with glutaminase (GLS) inhibitor 968 in PRC3/WT8 (A) and UMRC2 cells (B). Rescue of GLS inhibition with dimethyl alpha-ketoglutarate (DM-Akg; 4 mM) or acetate (4 mM) in PRC3/WT8 clonal cells (C) and polyclonal 786-O cells (D). Effect of GLS inhibitor BPTES in UMRC2 cells (E). Student's t test compares *VHL*-reconstituted cells to control cells in (A), (B), and (E) and DM-Akg or acetate-rescued cells to correspondent control cells treated with 968 only in (C) and (D) (asterisk in parenthesis indicates comparison between VHL-reconstituted to control cells). Error bars represent SEM.

(F) GLS inhibitor BPTES suppresses growth of human UMRC3 RCC cells as xenografts in nu/nu mice. When the tumors reached 100 mm^3, injections with BPTES or vehicle control were carried out daily for 14 days (n = 12). BPTES treatment decreases tumor size and mass (see insert). Student's t test compares control to BPTES-treated mice (F). Error bars represent SEM.

(G) Diagram showing the regulation of reductive carboxylation by HIF.

administration of acetate or citrate had a mild effect in VHL-positive cells. In the case of either cell type, the magnitude of changes in RC reflected the degree of changes in intracellular citrate levels. These observations show that fluctuations in citrate levels by HIF modulate, at least in part, the flux of the reverse IDH reaction. This finding underlines the compensatory role of RC in maintaining an adequate flux for lipogenesis under HIF-activated conditions.

In addition to the role of HIF in regulating RC through citrate, we examined whether HIF directly regulates enzymes along the reductive TCA cycle pathway (see Figure 1B). We did not observe changes in the transcript or protein levels of GLS, GDH, IDH1, IDH2, ACO1, or ATP citrate lyase between VHL-deficient and VHL-reconstituted UMRC2 cells. This is in line with previous studies that did not identify any of these enzymes as transcriptional targets of HIF-1α or HIF-2α (Mole et al., 2009; Ortiz-Barahona et al., 2010; Schödel et al., 2011; Wenger et al., 2005). Nevertheless, it is conceivable that HIF may affect the activity of these enzymes through regulation of cofactor availability or posttranslational modification of the enzymes. For example, the reverse IDH reaction requires NADPH, as allosteric cofactor (Dalziel and Londesborough, 1968; Leonardi et al., 2012) and HIF-mediated changes in NADPH levels may indirectly influence IDH activity. In our studies we did not observe increased NADPH levels in VHL-deficient cells when compared to the VHL-positive counterparts, which is in agreement with existing literature showing that HIF-1α activates NADPH oxidase and hypoxia limits NADPH production (Diebold et al., 2010; Tribble and Jones, 1990). These data suggest that the mass-action effect of HIF toward RC is not accounted for by an increase in NADPH production. Other signaling pathways may regulate RC through NADPH availability, and the source(s) of NADPH contributing to RC in the cytosol/mitochondrion are under investigation. For example, the mitochondrial enzyme nicotinamide nucleotide transhydrogenase (NNT) transfers reducing equivalents from NADH to NADPH and has been hypothesized to contribute to RC by IDH2 (Sazanov and Jackson, 1994). This hypothesis, although not yet experimentally tested, raises the possibility that NADPH-producing reactions may regulate the RC flux in a HIF-independent manner.

In addition, posttranslational modifications of the enzymes involved in RC may be influenced by hypoxia and/or HIF expression indirectly. For example, aconitase (ACO1) activity is reportedly regulated by hypoxia through iron-sulfur cluster modifications and phosphorylation (Chan et al., 2009; Rouault, 2006), and acetyl-CoA is a required substrate for protein acetylation, which regulates major cellular functions including central carbon metabolism (Wang et al., 2010b; Zhao et al., 2010). Thus, it is conceivable that HIF contributes to these modifications and therefore influences the activity of glutamine-metabolizing enzymes at the posttranslational level.

Our current work showed that HIF-2α is sufficient to induce the reductive program in RCC cells that express only the HIF-2α paralog, while mouse NEK cells appeared to use HIF-1α preferentially to promote RC. Together with the evidence that HIF-1α and HIF-2α may have opposite roles in tumor growth (Keith et al., 2011; Maranchie et al., 2002; Raval et al., 2005), it is possible that the cellular context dictates which paralog acti-

vates RC. It is also possible that HIF-2α adopts the RC regulatory function of HIF-1α upon deletion of the latter in RCC cells. Further studies are warranted in understanding the relative role of HIF-α paralogs in regulating RC in different cell types.

Finally, the selective sensitivity to glutaminase inhibitors exhibited by VHL-deficient cells, together with the observed RC activity in vivo, strongly suggests that reductive glutamine metabolism may fuel tumor growth. Investigating whether the reductive flux correlates with tumor hypoxia and/or contributes to the actual cell survival under low oxygen conditions is warranted. Together, our findings underscore the biological significance of reductive carboxylation in VHL-deficient RCC cells. Targeting this metabolic signature of HIF may open viable therapeutic opportunities for the treatment of hypoxic and VHL-deficient tumors.

EXPERIMENTAL PROCEDURES

Cell Culture and Metabolic Labeling

All cell lines were obtained from ATCC, tested for mycoplasma, and maintained in Dulbecco's modified Eagle's medium (DMEM; GIBCO-BRL) containing 10% FBS (HyClone) supplemented with penicillin-streptomycin (Invitrogen). Metabolic labeling was described before (Metallo et al., 2012).

Cellular Metabolite Extractions and GC-MS Analysis

The method was described before (Metallo et al., 2012). Briefly, metabolic activity was quenched with methanol ($-80°C$), an equal volume of water was added, and cells were collected in tubes by pipette scraping the wells. Two volumes of chloroform ($-20°C$) were added to each tube, extracts were vortexed and centrifuged at 11,000 RPM for 10 min at 4°C. The aqueous phase was used for polar metabolite analysis, and the chloroform phase was used for fatty acid analysis. Polar phase containing amino and organic acids was evaporated, dissolved in 2% methoxyamine hydrochloride in pyridine, derivatized by adding N-methyl-N-tert-butyldimethylsilyltrifluoroacetamide + 1% tert-butyldimethylchlorosilane, and subjected to GC-MS analysis. Fatty acid methyl esters (FAMEs) were obtained by reacting the nonpolar phase with 2% H_2SO_4:methanol. After transesterification, FAMEs were isolated by adding hexane and saturated NaCl. The hexane phase was subjected to GC-MS analysis.

Metabolic Flux Analysis and Isotopomer Spectral Analysis

Intracellular fluxes and the specific contribution to lipogenic acetyl-CoA were estimated using the elementary metabolite unit (EMU) framework-based software Metran, executed in Matlab (Mathworks) as previously described (Metallo et al., 2012).

Metabolite Analysis of Extracellular Medium

Cells were seeded at low density in basal DMEM and the spent medium was collected at the end of a 72 hr growth period and analyzed using a Yellow Springs Instruments (YSI) 7100.

Determination of NADP+/NADPH Ratios

Cellular NADP+/NADPH levels were assayed using a fluorescence-based assay according to the manufacturer's instructions (Cell Technology). NADP+/NADPH ratios were also determined employing the method developed in the Krebs lab, as described therein (Veech et al., 1969).

Plasmids and Western Blots

Plasmids expressing HA-VHL mutants and HA-HIF-2α were purchased from Addgene. Plasmids encoding shRNA sequences targeting PDK1 and ACLY were obtained from the Broad Institute RNAi Consortium (TRC) library available at Massachusetts General Hostpital (MGH) (shRNA sequences available in the Supplemental Experimental Procedures). Proteins were extracted and immunoblotted as described before (Zimmer et al., 2008).

Animal Studies

All protocols conformed to institutional regulations. UMRC3 cells were injected subcutaneously in nu/nu mice (5×10^6 cells per injection). Tumor volumes were calculated as length (mm) × width^2 (mm^2) × 0.5. For in vivo ^{13}C-labeling studies, animals (n = 3) were infused with [1-^{13}C$_1$]glutamine for the indicated time periods as previously described (Marin-Valencia et al., 2012).

^{13}C NMR Spectroscopy

High-resolution proton-decoupled ^{13}C NMR spectra of tumor extracts were obtained at 11.7 T (125.13 Hz, 25°C [pH 7.2]) in a Bruker AVANCE III 500 MHz Wide Bore NMR spectrometer using a commercial (5 mm) triple-resonance probe (^{1}H, ^{13}C, ^{2}H) optimized for direct ^{13}C detection.

Statistical Analysis

For MFA and ISA results, error bars represent 95% confidence intervals. In all other experiments, error bars represent SEM unless otherwise noted. Statistical significance was determined using two-tailed Student's t test. *$p < 0.05$, **$p < 0.001$.

SUPPLEMENTAL INFORMATION

Supplemental Information includes four figures, one table, and Supplemental Experimental Procedures and can be found with this article online at http://dx.doi.org/10.1016/j.cmet.2013.02.002.

REFERENCES

Cairns, R.A., Harris, I.S., and Mak, T.W. (2011). Regulation of cancer cell metabolism. Nat. Rev. Cancer 11, 85–95.

Chan, S.Y., Zhang, Y.Y., Hemann, C., Mahoney, C.E., Zweier, J.L., and Loscalzo, J. (2009). MicroRNA-210 controls mitochondrial metabolism during hypoxia by repressing the iron-sulfur cluster assembly proteins ISCU1/2. Cell Metab. 10, 273–284.

Chitalia, V.C., Foy, R.L., Bachschmid, M.M., Zeng, L., Panchenko, M.V., Zhou, M.I., Bharti, A., Seldin, D.C., Lecker, S.H., Dominguez, I., and Cohen, H.T. (2008). Jade-1 inhibits Wnt signalling by ubiquitylating beta-catenin and mediates Wnt pathway inhibition by pVHL. Nat. Cell Biol. 10, 1208–1216.

Dalziel, K., and Londesborough, J.C. (1968). The mechanisms of reductive carboxylation reactions. Carbon dioxide or bicarbonate as substrate of nicotinamide-adenine dinucleotide phosphate-linked isocitrate dehydrogenase and malic enzyme. Biochem. J. 110, 223–230.

DeBerardinis, R.J., and Cheng, T. (2010). Q's next: the diverse functions of glutamine in metabolism, cell biology and cancer. Oncogene 29, 313–324.

Diebold, I., Petry, A., Hess, J., and Görlach, A. (2010). The NADPH oxidase subunit NOX4 is a new target gene of the hypoxia-inducible factor-1. Mol. Biol. Cell 21, 2087–2096.

Ebert, B.L., Gleadle, J.M., O'Rourke, J.F., Bartlett, S.M., Poulton, J., and Ratcliffe, P.J. (1996). Isoenzyme-specific regulation of genes involved in energy metabolism by hypoxia: similarities with the regulation of erythropoietin. Biochem. J. 313, 809–814.

Filipp, F.V., Scott, D.A., Ronai, Z.A., Osterman, A.L., and Smith, J.W. (2012). Reverse TCA cycle flux through isocitrate dehydrogenases 1 and 2 is required for lipogenesis in hypoxic melanoma cells. Pigment Cell Melanoma Res 25, 375–383.

Firth, J.D., Ebert, B.L., Pugh, C.W., and Ratcliffe, P.J. (1994). Oxygen-regulated control elements in the phosphoglycerate kinase 1 and lactate dehydrogenase A genes: similarities with the erythropoietin 3′ enhancer. Proc. Natl. Acad. Sci. USA 91, 6496–6500.

Gordan, J.D., and Simon, M.C. (2007). Hypoxia-inducible factors: central regulators of the tumor phenotype. Curr. Opin. Genet. Dev. 17, 71–77.

Hatzivassiliou, G., Zhao, F., Bauer, D.E., Andreadis, C., Shaw, A.N., Dhanak, D., Hingorani, S.R., Tuveson, D.A., and Thompson, C.B. (2005). ATP citrate lyase inhibition can suppress tumor cell growth. Cancer Cell 8, 311–321.

Iyer, N.V., Kotch, L.E., Agani, F., Leung, S.W., Laughner, E., Wenger, R.H., Gassmann, M., Gearhart, J.D., Lawler, A.M., Yu, A.Y., and Semenza, G.L. (1998). Cellular and developmental control of O2 homeostasis by hypoxia-inducible factor 1 alpha. Genes Dev. 12, 149–162.

Keith, B., Johnson, R.S., and Simon, M.C. (2011). HIF1α and HIF2α: sibling rivalry in hypoxic tumour growth and progression. Nat. Rev. Cancer 12, 9–22.

Kim, W., and Kaelin, W.G., Jr. (2003). The von Hippel-Lindau tumor suppressor protein: new insights into oxygen sensing and cancer. Curr. Opin. Genet. Dev. 13, 55–60.

Kim, J.W., Tchernyshyov, I., Semenza, G.L., and Dang, C.V. (2006). HIF-1-mediated expression of pyruvate dehydrogenase kinase: a metabolic switch required for cellular adaptation to hypoxia. Cell Metab. 3, 177–185.

Lehninger, A.L. (2005). The Citric Acid Cycle. In Lehninger Principles of Biochemistry, 4th edition, D.L. Nelson and M.M. Cox, eds. (New York: W.H. Freeman and Company), pp. 621–622.

Leonardi, R., Subramanian, C., Jackowski, S., and Rock, C.O. (2012). Cancer-associated isocitrate dehydrogenase mutations inactivate NADPH-dependent reductive carboxylation. J. Biol. Chem. 287, 14615–14620.

Li, L., Zhang, L., Zhang, X., Yan, Q., Minamishima, Y.A., Olumi, A.F., Mao, M., Bartz, S., and Kaelin, W.G., Jr. (2007). Hypoxia-inducible factor linked to differential kidney cancer risk seen with type 2A and type 2B VHL mutations. Mol. Cell. Biol. 27, 5381–5392.

Luo, W., Hu, H., Chang, R., Zhong, J., Knabel, M., O'Meally, R., Cole, R.N., Pandey, A., and Semenza, G.L. (2011). Pyruvate kinase M2 is a PHD3-stimulated coactivator for hypoxia-inducible factor 1. Cell 145, 732–744.

Maranchie, J.K., Vasselli, J.R., Riss, J., Bonifacino, J.S., Linehan, W.M., and Klausner, R.D. (2002). The contribution of VHL substrate binding and HIF1-alpha to the phenotype of VHL loss in renal cell carcinoma. Cancer Cell 1, 247–255.

Marin-Valencia, I., Yang, C., Mashimo, T., Cho, S., Baek, H., Yang, X.L., Rajagopalan, K.N., Maddie, M., Vemireddy, V., Zhao, Z., et al. (2012). Analysis of tumor metabolism reveals mitochondrial glucose oxidation in genetically diverse human glioblastomas in the mouse brain in vivo. Cell Metab. 15, 827–837.

Melvin, A., and Rocha, S. (2012). Chromatin as an oxygen sensor and active player in the hypoxia response. Cell. Signal. 24, 35–43.

Metallo, C.M., Gameiro, P.A., Bell, E.L., Mattaini, K.R., Yang, J., Hiller, K., Jewell, C.M., Johnson, Z.R., Irvine, D.J., Guarente, L., et al. (2012). Reductive glutamine metabolism by IDH1 mediates lipogenesis under hypoxia. Nature 481, 380–384.

Mikhaylova, O., Ignacak, M.L., Barankiewicz, T.J., Harbaugh, S.V., Yi, Y., Maxwell, P.H., Schneider, M., Van Geyte, K., Carmeliet, P., Revelo, M.P., et al. (2008). The von Hippel-Lindau tumor suppressor protein and Egl-9-Type proline hydroxylases regulate the large subunit of RNA polymerase II in response to oxidative stress. Mol. Cell. Biol. 28, 2701–2717.

Mole, D.R., Blancher, C., Copley, R.R., Pollard, P.J., Gleadle, J.M., Ragoussis, J., and Ratcliffe, P.J. (2009). Genome-wide association of hypoxia-inducible factor (HIF)-1alpha and HIF-2alpha DNA binding with expression profiling of hypoxia-inducible transcripts. J. Biol. Chem. 284, 16767–16775.

Mullen, A.R., Wheaton, W.W., Jin, E.S., Chen, P.H., Sullivan, L.B., Cheng, T., Yang, Y., Linehan, W.M., Chandel, N.S., and DeBerardinis, R.J. (2012).

Reductive carboxylation supports growth in tumour cells with defective mitochondria. Nature 481, 385–388.

Ohh, M., Yauch, R.L., Lonergan, K.M., Whaley, J.M., Stemmer-Rachamimov, A.O., Louis, D.N., Gavin, B.J., Kley, N., Kaelin, W.G., Jr., and Iliopoulos, O. (1998). The von Hippel-Lindau tumor suppressor protein is required for proper assembly of an extracellular fibronectin matrix. Mol. Cell 1, 959–968.

Ortiz-Barahona, A., Villar, D., Pescador, N., Amigo, J., and del Peso, L. (2010). Genome-wide identification of hypoxia-inducible factor binding sites and target genes by a probabilistic model integrating transcription-profiling data and in silico binding site prediction. Nucleic Acids Res. 38, 2332–2345.

Papandreou, I., Cairns, R.A., Fontana, L., Lim, A.L., and Denko, N.C. (2006). HIF-1 mediates adaptation to hypoxia by actively downregulating mitochondrial oxygen consumption. Cell Metab. 3, 187–197.

Raval, R.R., Lau, K.W., Tran, M.G., Sowter, H.M., Mandriota, S.J., Li, J.L., Pugh, C.W., Maxwell, P.H., Harris, A.L., and Ratcliffe, P.J. (2005). Contrasting properties of hypoxia-inducible factor 1 (HIF-1) and HIF-2 in von Hippel-Lindau-associated renal cell carcinoma. Mol. Cell. Biol. 25, 5675–5686.

Roe, J.S., Kim, H., Lee, S.M., Kim, S.T., Cho, E.J., and Youn, H.D. (2006). p53 stabilization and transactivation by a von Hippel-Lindau protein. Mol. Cell 22, 395–405.

Rouault, T.A. (2006). The role of iron regulatory proteins in mammalian iron homeostasis and disease. Nat. Chem. Biol. 2, 406–414.

Sazanov, L.A., and Jackson, J.B. (1994). Proton-translocating transhydrogenase and NAD- and NADP-linked isocitrate dehydrogenases operate in a substrate cycle which contributes to fine regulation of the tricarboxylic acid cycle activity in mitochondria. FEBS Lett. 344, 109–116.

Schödel, J., Oikonomopoulos, S., Ragoussis, J., Pugh, C.W., Ratcliffe, P.J., and Mole, D.R. (2011). High-resolution genome-wide mapping of HIF-binding sites by ChIP-seq. Blood 117, e207–e217.

Semenza, G.L. (2010). HIF-1: upstream and downstream of cancer metabolism. Curr. Opin. Genet. Dev. 20, 51–56.

Thoma, C.R., Frew, I.J., Hoerner, C.R., Montani, M., Moch, H., and Krek, W. (2007). pVHL and GSK3beta are components of a primary cilium-maintenance signalling network. Nat. Cell Biol. 9, 588–595.

Tribble, D.L., and Jones, D.P. (1990). Oxygen dependence of oxidative stress. Rate of NADPH supply for maintaining the GSH pool during hypoxia. Biochem. Pharmacol. 39, 729–736.

Veech, R.L., Eggleston, L.V., and Krebs, H.A. (1969). The redox state of free nicotinamide-adenine dinucleotide phosphate in the cytoplasm of rat liver. Biochem. J. 115, 609–619.

Wang, J.B., Erickson, J.W., Fuji, R., Ramachandran, S., Gao, P., Dinavahi, R., Wilson, K.F., Ambrosio, A.L., Dias, S.M., Dang, C.V., and Cerione, R.A. (2010a). Targeting mitochondrial glutaminase activity inhibits oncogenic transformation. Cancer Cell 18, 207–219.

Wang, Q., Zhang, Y., Yang, C., Xiong, H., Lin, Y., Yao, J., Li, H., Xie, L., Zhao, W., Yao, Y., et al. (2010b). Acetylation of metabolic enzymes coordinates carbon source utilization and metabolic flux. Science 327, 1004–1007.

Wenger, R.H., Stiehl, D.P., and Camenisch, G. (2005). Integration of oxygen signaling at the consensus HRE. Sci. STKE 2005, re12.

Wise, D.R., Ward, P.S., Shay, J.E., Cross, J.R., Gruber, J.J., Sachdeva, U.M., Platt, J.M., DeMatteo, R.G., Simon, M.C., and Thompson, C.B. (2011). Hypoxia promotes isocitrate dehydrogenase-dependent carboxylation of α-ketoglutarate to citrate to support cell growth and viability. Proc. Natl. Acad. Sci. USA 108, 19611–19616.

Yang, H., Minamishima, Y.A., Yan, Q., Schlisio, S., Ebert, B.L., Zhang, X., Zhang, L., Kim, W.Y., Olumi, A.F., and Kaelin, W.G., Jr. (2007). pVHL acts as an adaptor to promote the inhibitory phosphorylation of the NF-kappaB agonist Card9 by CK2. Mol. Cell 28, 15–27.

Yoo, H., Stephanopoulos, G., and Kelleher, J.K. (2004). Quantifying carbon sources for de novo lipogenesis in wild-type and IRS-1 knockout brown adipocytes. J. Lipid Res. 45, 1324–1332.

Zhao, S., Xu, W., Jiang, W., Yu, W., Lin, Y., Zhang, T., Yao, J., Zhou, L., Zeng, Y., Li, H., et al. (2010). Regulation of cellular metabolism by protein lysine acetylation. Science 327, 1000–1004.

Zhong, Z., Arteel, G.E., Connor, H.D., Yin, M., Frankenberg, M.V., Stachlewitz, R.F., Raleigh, J.A., Mason, R.P., and Thurman, R.G. (1998). Cyclosporin A increases hypoxia and free radical production in rat kidneys: prevention by dietary glycine. Am. J. Physiol. 275, F595–F604.

Zimmer, M., Ebert, B.L., Neil, C., Brenner, K., Papaioannou, I., Melas, A., Tolliday, N., Lamb, J., Pantopoulos, K., Golub, T., and Iliopoulos, O. (2008). Small-molecule inhibitors of HIF-2a translation link its 5'UTR iron-responsive element to oxygen sensing. Mol. Cell 32, 838–848.